Harmonic Domain Modelling of Transformer Core Nonlinearities Using the DIgSILENT PowerFactory Software

Bak, Claus Leth; Bak-Jensen, Birgitte; Wiechowski, Wojciech

Published in:
Jakosc i Uzytkowanie Energii Elektrycznej

Publication date:
2008

Document Version
Publisher's PDF, also known as Version of record

Harmonic Domain Modelling of Transformer Core Nonlinearities Using the DIgSILENT PowerFactory Software

Wojciech WIECHOWSKI [1], Birgitte BAK-JENSEN [2], Claus LETH BAK [2], Jan LYKKEGAARD [1]

1) Danish TSO Energinet.dk; Denmark

2) Aalborg University, Denmark

Summary: **This paper demonstrates the results of implementation and verification of an already existing algorithm that allows for calculating saturation characteristics of single-phase power transformers. The algorithm was described for the first time in 1993. Now this algorithm has been implemented using the DIgSILENT Programming Language (DPL) as an external script in the harmonic domain calculations of a power system analysis tool PowerFactory [10]. The algorithm is verified by harmonic measurements on a single-phase power transformer. A theoretical analysis of the core nonlinearities phenomena in single and three-phase transformers is also presented. This analysis leads to the conclusion that the method can be applied for modelling nonlinearities of three-phase autotransformers.**

Key words:
autotransformers, harmonic analysis, nonlinearities, simulation software, transformer cores

1. INTRODUCTION

In harmonic analysis studies, power transformers can be either modelled as linear power system components, or using more sophisticated models that take into account the iron core nonlinearity and its property of distorting currents resulting in an "injection" of harmonic currents into the network. If the transformer core is to be modelled as an impedance, it is sufficient to model the iron core as a shunt linear inductance and a resistance, connected in parallel. In order to model the nonlinear behaviour of the core, voltage dependence of an equivalent inductance and resistance shall be also included. Presented in this paper modelling of nonlinear cores of power transformers is a part of a larger project, where an existing computer model of the western grid of the Danish TSO Energinet.dk is to be adjusted for harmonic analysis purposes. Besides all linear power system components, special focus is attached to moidelling fo the nonlinearities present on the transmission level: converters of HVDC links and power transformers/autotransformers.

In order to minimize the core size, power transformers are usually designed to operate just below the knee point. Therefore, when the voltage increases above a certain value, the transformer magnetising current becomes distorted; even at the nominal operating voltage the no-load current THD can be as high as 20 % [4]. The harmonic contribution from power transformers can be most likely noticed in a grid with many transformers installed, during low load hours, when the load current is low and the voltage rises [4].

DIgSILENT PowerFactory enables to precisely model transformer core nonlinearity in the time domain (EMT) [8]. In the frequency domain it is not possible to do it so far. Since the frequency domain is more convenient for harmonic analysis than EMT, an attempt was made to model transformer core nonlinearity in the harmonic domain calculations of PowerFactory. Several ways of modelling the iron core nonlinearities exist, described for instance in [5, 9 or 2]. These methods require that the dynamic hysteresis loops of the material are known. This is not always possible, especially if the nonlinearities of older transformers are of interest. In this project the only data available for the autotransformers are typical test reports. Therefore, a different method has been found, where the core nonlinearities can be determined using a simpler set of input data [7]. For computation, the method requires only $V_{rms} - I_{rms}$ curves and the no-load losses at fundamental frequency. These data are present in the test reports. The method was implemented as an external script of DIgSILENT PowerFactory using the DIgSILENT Programming Language (DPL). The implementation of the method and its verification is illustrated. It is also shown that the method is applicable for modelling nonlinearities of power autotransformers.

2. THEORY

In an iron-core power transformer, the flux Φ and the flux density B within the transformer core is proportional to the voltage u_1 applied across the primary winding, according to the Faraday's law. In the sinusoidal case it can be written [1]:

$$u_1 = U_{1m} \sin \omega t = \frac{d\phi}{dt} \tag{1}$$

$$\phi = \int U_{1m} \sin \omega t \, dt = \frac{U_{1m}}{\omega} \cos \omega t = \Phi_m \cos \omega t \tag{2}$$

$$B = \frac{\phi}{S} = \frac{\int U_{1m} \sin \omega t \, dt}{S} \tag{3}$$

where S is the cross-section of the core.

The resultant magnetizing current I_m needed to produce this sinusoidal flux is related to the magnetic field strength

H by a constant value, which is the ratio of number of turns N to the total length of the magnetic path l:

$$H = I\frac{N}{l} \tag{4}$$

The magnetic flux density B is related to the magnetic field strength H by the magnetic permeability of the steel used in the transformer core μ:

$$B = \mu H \tag{5}$$

Equation 5 shows that if the magnetic permeability μ is linear and B is sinusoidal, the magnetic field strength H (and what follows, the magnetizing current I_m) will be sinusoidal. If the transformer operates in saturation, μ is no longer linear and the magnetic field strength H is nonsinusoidal, because the product of H with the magnetic permeability μ must still produce the sinusoidal flux density B, see Figure 1. If the magnetizing current I_m is allowed to flow freely (low impedance path $\boldsymbol{Z}$ for all harmonics), after decomposing it to Fourier components, it will contain the fundamental frequency and all the odd harmonics: 3rd, 5th, 7th,9th etc [1].

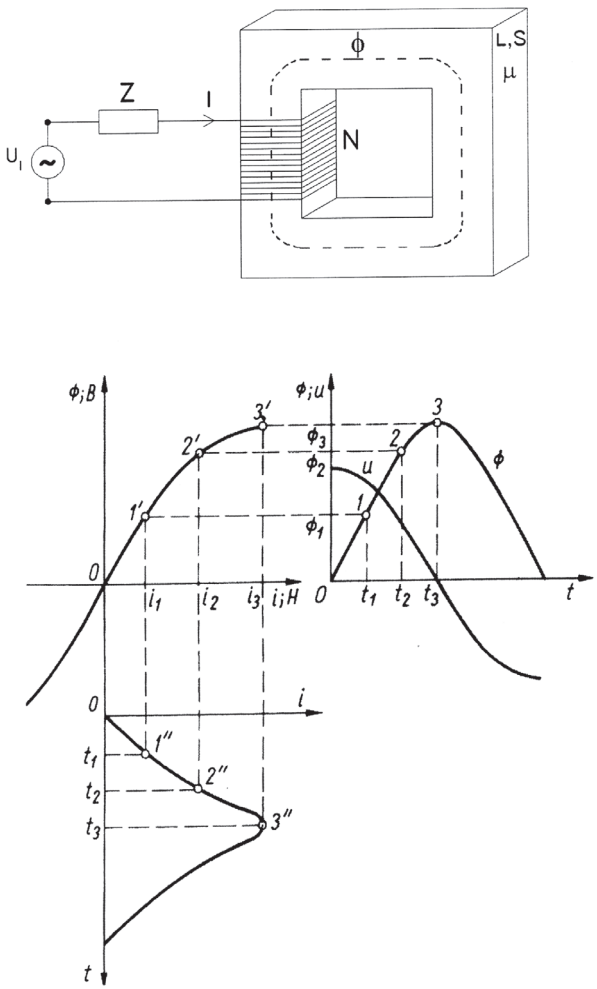

Fig. 1. Typical relations between main flux Φ, supplying voltage U and no-load (magnetizing) current I (without hysteresis effects) [6]

3. THE ALGORITHM AND ITS IMPLEMENTATION

In order to determine the magnetizing current harmonics, a special algorithm has been implemented [7]. Initially this technique was proposed in [3] for estimating the magnetizing inductance L_m. Reference [7] extended this algorithm with computation of the nonlinear resistance R_{Fe} (see Figure 2a). The main advantage of this algorithm is that both the equivalent resistance R_{Fe} and inductance L_m are calculated directly from the conventional transformer no-load test data: $V_{rms} - I_{rms}$ curve and the no-load losses at fundamental frequency. The nonlinear resistance (piecewise linear u-i_R characteristic) accounts for two effects: linear eddy current loss and nonlinear hysteresis loss. This resistance is found from the measured total no-load losses. Calculated in this way the resistive part of the total, measured no-load current can be subtracted geometrically. This allows for a calculation of the current flowing through the nonlinear inductance (piecewise linear λ–i_L characteristic). Next, the resulting, real and imaginary harmonic components are geometrically added and modelled as a current source. During harmonic load flow calculations, this current source will inject harmonic currents into the investigated network (Figure 2b).

The algorithm requires that the following assumptions and simplifications are made:

— winding impedances are ignored,
— supplying voltage and resulting flux are sinusoidal,
— the piecewise resistance and piecewise inductance are both symmetric.

The algorithm has been implemented in a dedicated simulation software DIgSILENT PowerFactory (PF). PowerFactory allows for creating automatic simulation tasks and build miscellaneous models of power system components, as the program possesses its own programming language DPL (DIgSILENT Programming Language). The syntax of this language is similar to C++. This language was used to implement the described algorithm. The basic idea was that the whole algorithm was programmed as several DLP subroutines and a main DPL controlling script. The structure of the algorithm implemented in PF is shown in Figure 3, and individual components of the algorithm are described in the following sections. Special emphasis is put

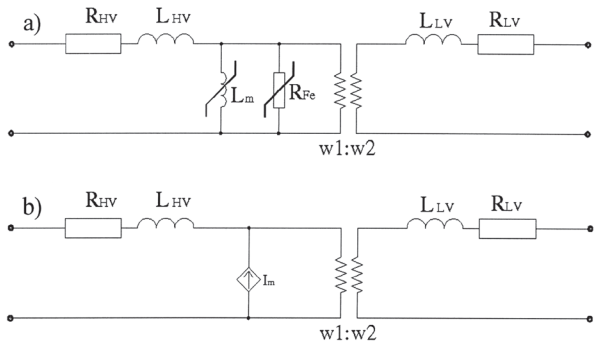

Fig. 2. Equivalent diagram of a power transformer: R_{HV}, R_{LV} – winding resistances, L_{HV}, L_{LV} – Leakage inductances; a) R_{Fe} – magnetizing resistance – hysteresis losses and eddy current losses in the core, L_m – magnetizing inductance; b) In the harmonic domain, nonlinearities are modelled as current source; I_m – magnetizing current

on the implementation details, and calculated, ready-to-use equations.

3.1. Routine Main

The main script *Main* (see Fig. 3), when executed recalculates all input data stored in the Data matrix (U_m, I_m) to the peak values and stores them in the matrix of results 'Results'. Letter m denotes the number of available measurements stored in Data. Next, the script automatically connects a current source to the HV transformer bus. Then it initiates conventional load-flow calculations. As a result of the load-flow, the three-phase voltages at the transformer bus are obtained. Next, the script Main executes in turn all the subroutines, beginning with subroutine *volt_comp*.

3.2. Subroutine volt_comp

This subroutine compares the calculated terminal voltages with the voltages stored in *Data* matrix and returns the row number *f* of the closest voltage value. If the bus voltage is higher than the highest voltage in the input data, the subroutine returns the max number of rows $f = m$. This means that the distorted magnetizing current will be constant for higher voltage values. This shall not be problematic during normal operation, since the voltage in no-load tests is usually varied up to 1.1 Un. When Subroutine *volt_comp* is accomplished, main script executes the next subroutine iR.

3.3. Subroutine iR

This subroutine calculates the first linear and next piecewise linear elements of the nonlinear resistance curve *R*. It is done in the following way. For the first segment, i.e. up to the first measured voltage, the peak current and the first linear segment of the resistance curve is calculated directly from input data:

$$P_1 = V_{rms_1} I_{r-rms_1} \tag{6}$$

$$I_{r_1} = \frac{2P_1}{V_1} \tag{7}$$

$$R_1 = \frac{V_1}{I_{r_1}} \tag{8}$$

The power measured at higher voltage values is a product of the sinusoidal voltage and nonsinusoidal current I_m (see Fig. 4). It can be seen that if linear resistance determined by (8) is used, the resultant current would be sinusoidal, regardless of the amplitude of the applied voltage. The peak value of this current would be much lower than in reality. Therefore, in order to assess the real current and the next segments of the piecewise linear curve, the power definition must be used:

$$P = \frac{2}{\pi}\int_0^{\frac{\pi}{2}} v(\alpha) i_r(\alpha) d\alpha \tag{9}$$

It is sufficient to calculate the current shape for ¼ of a period because the voltage is assumed sinusoidal. Therefore, the resultant current will contain only odd harmonic components and therefore, will be symmetrical.

The applied voltage can be written as $v(\alpha) = V_k \sin(\alpha)$. The total no-load power loss:

$$P_k = \frac{2}{\pi}\left[\begin{array}{l}\int_0^{\alpha_1}(V_k \sin\alpha)\left(\frac{V_k \sin\alpha}{R_1}\right)d\alpha + \\ \int_{\alpha_1}^{\alpha_2}(V_k \sin\alpha)\left(I_{r_1} + \frac{V_k \sin\alpha - V_1}{R_2}\right)d\alpha + \ldots + \\ \int_{\alpha_{k-1}}^{\frac{\pi}{2}}(V_k \sin\alpha)\left(I_{r_{k-1}} + \frac{V_k \sin\alpha - V_{k-1}}{R_k}\right)d\alpha\end{array}\right] \tag{10}$$

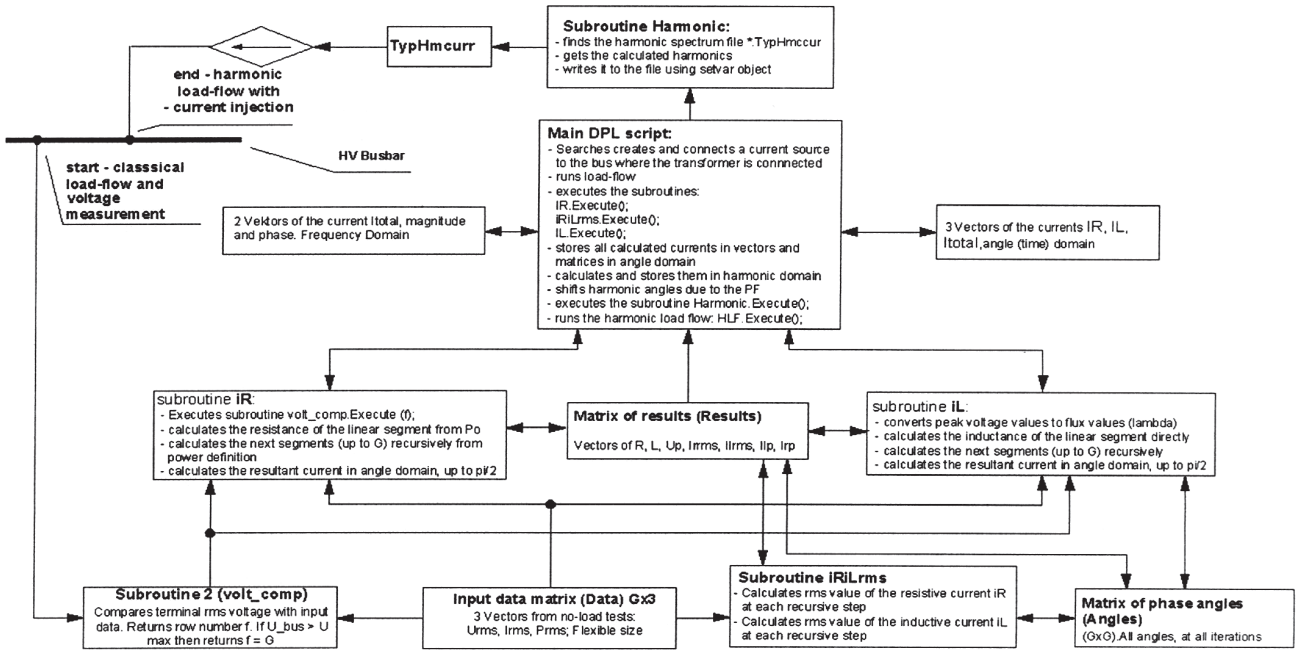

Fig. 3. Detailed structure of the implemented algorithm

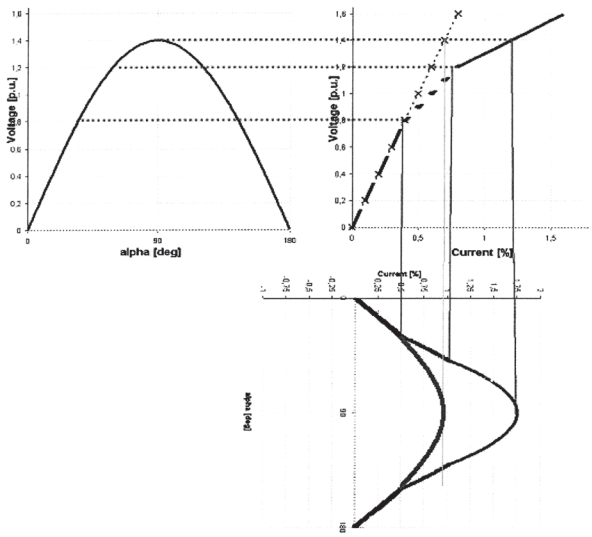

Fig. 4. Sinusoidal voltage applied to the piecewise linear v-I_R curve and the resultant, approximated nonlinear current

The angles $\alpha_1, \alpha_2, ..., \alpha_{k-1}$ are calculated from $\alpha_j = \arcsin(V_j/V_k), j = 1, 2, ..., k-1$ and stored at each recursive step in the matrix of phase angles *Angles*. The computation using (10) must be done recursively — segment by segment. The part of (10) that is underlined with a single line shall be recomputed at each recursive step, because the voltage V_k must be updated. Part of (10) underlined with double line must be updated and computed recursively for each segment up to the last segment where α reaches $\pi/2$. For instance to calculate (10) for $k = 3$, there would be 3 unknowns: R_2, I_{r2} and R_3, and only one equation. Therefore, first it is necessary to compute (10) for $k = 2$. Then the only unknown is R_2 so it can be computed. Equation 10 can be rewritten in the form from which it is easy to determine the unknown value of resistance:

$$P_k = a_{r_k} + \frac{b_{r_k}}{R_k} \quad \Rightarrow \; R_k = \frac{b_{r_k}}{P_k - a_{r_k}} \tag{11}$$

Components a_{r_k} and b_{r_k} were computed and are given below in a ready-to-use fashion:

$$a_{r_k} = \frac{2}{\pi}\left[\frac{V_{(k)}^2}{R_1}\left(\frac{1}{2}\alpha_1 - \frac{\cos\alpha_1 \sin\alpha_1}{2}\right) + \underline{\underline{V_{(k)} I_{r(k-1)}\left(\cos\alpha_{(k-1)} - \cos\alpha_{(k)}\right)}}\right] \tag{12}$$

$$b_{r_k} = \frac{2}{\pi}\left[\frac{\frac{V_{(k)}^2}{2}\left(\begin{array}{l}\cos\alpha_{(k-1)}\sin\alpha_{(k-1)} - \cos\alpha_k \sin\alpha_k \\ +\alpha_k - \alpha_{(k-1)}\end{array}\right) -}{\underline{\underline{-V_{(k)} V_{(k-1)}\left(\cos\alpha_{(k-1)} - \cos\alpha_{(k)}\right)}}}\right] \tag{13}$$

Next, the subroutine *iR* must calculate the current I_{r2} from:

$$I_{r_k} = I_{r_{k-1}} + \frac{V_k - V_{k-1}}{R_k} \tag{14}$$

When R_2 and I_{r2} is known, the calculations can be started again, now for $k = 3$, to determine R_3. This procedure is repeated for each segment (each voltage in the *Data* matrix) except for the first one, i.e. for $k \geq 2$. Resistance R and current peak I_{rk} values are stored in the matrix *Results*.

3.4. Subroutine *iL*

The λ–i_1 curve is calculated by the Subroutine *iL*. Peak flux values λ_k are related to the peak voltage values V_k by the expression [7]:

$$\lambda_k = \frac{V_k}{\varpi} \tag{15}$$

where I_{t-rmsk} is the total measured rms no-load current, I_{r-rmsk} is the determined in previous section rms resistive current component and I_{l-rmsk} is the inductive rms current component to be computed. For the first segment in the λ–i_l curve subroutine *iL* calculates the assumed linear inductance using equations:

$$I_{l_1} = I_{l-rms_1}\sqrt{2} \tag{16}$$

$$\lambda_1 = \frac{V_1}{\varpi} \tag{17}$$

$$L = \frac{\lambda_1}{I_{l_1}} = \frac{V_1}{\varpi I_{l_1}} \tag{18}$$

For segments k ≥ 2, assuming $\lambda_k(\alpha) = \lambda_k \sin(\alpha)$, rms definition for the current will be:

$$I_{l-rms_k}^2 = \frac{2}{\pi}\left[\begin{array}{l}\underline{\int_0^{\alpha_1}\left(\frac{\lambda_k \sin\alpha}{L_1}\right)d\alpha + \int_{\alpha_1}^{\alpha_2}\left(\frac{I_{l_1} + \lambda_k \sin\alpha - \lambda_1}{L_2}\right)d\alpha + \ldots +} \\ \underline{\underline{\int_{\alpha_{k-1}}^{\frac{\pi}{2}}\left(I_{l_{k-1}} + \frac{\lambda_k \sin\alpha - \lambda_{k-1}}{L_k}\right)d\alpha}}\end{array}\right] \tag{19}$$

This equation is analogous to (10), i.e. it must be computed segment by segment. This equation can be rewritten in the form:

$$a_{lk}\left(\frac{1}{L_k}\right)^2 + b_{lk}\left(\frac{1}{L_k}\right) + \left(c_{lk} + x_0\right) = 0 \tag{20}$$

For this quadratic equation it is assumed [7] that $a_{lk} > 0$, $b_{lk} > 0$ and $(c_{lk} + x_0) < 0$. Therefore, the linear segments of the inductance L_k are calculated from:

$$L_k = \frac{2a_{lk}}{-b_{lk} + \sqrt{b_{lk}^2 - 4a_{lk}\left(c_{lk} + x_0\right)}} \tag{21}$$

Components $a_{L_k}, b_{L_k}, c_{L_k}, x_0$ were computed and are given below in a ready-to-use fashion:

$$x_0 = \frac{\lambda_k^2}{L_1^2}\left[\begin{array}{l}\dfrac{\cos\alpha_{(k-1)}\sin\alpha_{(k-1)}}{2} - \dfrac{\cos\alpha_{(k)}\sin\alpha_{(k)}}{2} + \\ \dfrac{\alpha_{(k)} - \alpha_{(k-1)}}{2}\end{array}\right] \quad (22)$$

$$a_{lk} = \left[\begin{array}{l}-\lambda_{(k)}^2 \cdot x_1 + \lambda_{(n-1)}^2\left(\alpha_{(n)} - \alpha_{(n-1)}\right) + \\ 2\lambda_{(k)}\lambda_{(n-1)}\left(\cos\alpha_{(n-1)} - \cos\alpha_{(n)}\right)\end{array}\right] \quad (23)$$

$$x_1 = \left[\begin{array}{l}\dfrac{\cos\alpha_{(n-1)}\sin\alpha_{(n-1)}}{2} - \dfrac{\cos\alpha_{(n)}\sin\alpha_{(n)}}{2} + \\ \dfrac{\alpha_{(n)} - \alpha_{(n-1)}}{2}\end{array}\right] \quad (24)$$

$$b_{lk} = \left[\begin{array}{l}-2\lambda_{(k)} I_{L_{(n-1)}}\left(\cos\alpha_{(n-1)} - \cos\alpha_{(n)}\right) + \\ 2\lambda_{(n-1)} I_{L_{(n-1)}}\left(\alpha_{(n)} - \alpha_{(n-1)}\right)\end{array}\right] \quad (25)$$

$$c_{lk} = \left[-I_{L_{(n-1)}}^2\left(\alpha_{(n)} - \alpha_{(n-1)}\right)\right] \quad (26)$$

and the peak current I_{lk} must be also computed at each segment from:

$$i_{l_k} = i_{l_{k-1}} + \frac{1}{L_k}\left(\lambda_k - \lambda_{k-1}\right) \quad (27)$$

4.5. Subroutine *iRiLrms*

This subroutine calculates the *rms* value of the distorted resistive current component I_{rkrms} and later, the *rms* value distorted inductive component I_{Lkrms}, at each recursive step. The *rms* value of the resistive current I_{rkrms} is found from the *rms* definition:

$$I_{rms}^2 = \frac{2}{\pi}\int_0^{\frac{\pi}{2}} i^2(\alpha)\, d\alpha \quad (28)$$

$$I_{r-rms_k}^2 = \frac{2}{\pi}\left[\begin{array}{l}\displaystyle\int_0^{\alpha_1}\left(\frac{V_k \sin\alpha}{R_1}\right)^2 d\alpha + \\ \displaystyle\int_{\alpha_1}^{\alpha_2}\left(I_{r_1} + \frac{V_k \sin\alpha - V_1}{R_2}\right)^2 d\alpha + \ldots + \\ \displaystyle\int_{\alpha_{k-1}}^{\frac{\pi}{2}}\left(I_{r_{k-1}} + \frac{V_k \sin\alpha - V_{k-1}}{R_k}\right)^2 d\alpha\end{array}\right] \quad (29)$$

Equation 29 is given below in a ready-to-use fashion:

$$I_{r-rms_k}^2 = \frac{2}{\pi}\left[\begin{array}{l}\dfrac{V_k^2}{R_1^2}\left(-\dfrac{\cos\alpha_{(1,k)}\sin\alpha_{(1,k)}}{2} + \dfrac{\alpha_{(1,k)}}{2}\right) + \\ \dfrac{V_k^2}{R_n^2}\left(\dfrac{\cos\alpha_{(n-1,k)}\sin\alpha_{(n-1,k)}}{2} - \right. \\ \left.\dfrac{\cos\alpha_{(n,k)}\sin\alpha_{(n,k)}}{2} + \dfrac{\alpha_{(n,k)} - \alpha_{(n-1,k)}}{2}\right) + \\ \left(2I_{r_{(n-1)}}\dfrac{V_{(k)}}{R_{(n)}} - 2\dfrac{V_{(k)}V_{(n-1)}}{R_n^2}\right)\left(\begin{array}{l}-\cos\alpha_{(n-1,k)} - \\ \cos\alpha_{(n,k)}\end{array}\right) + \\ \left(I^2{}_{r_{(n-1)}} - 2I_{r_{(n-1)}}\dfrac{V_{(n-1)}}{R_{(n)}} + \dfrac{V_{(n-1)}^2}{R_{(n)}^2}\right)\left(-\alpha_{(n)} - \alpha_{(n-1)}\right)\end{array}\right] \quad (30)$$

If sinusoidal voltage is applied to the parallel connection of linear inductance and resistance, the resistive current will be in phase with the applied voltage and inductive current will be shifted by 90°. In case of nonlinear resistance and inductance, the resistive and reactive currents will be distorted, i.e. they will contain harmonics but still the adequate harmonic components will be orthogonal with respect to each other [7]. Based on this assumption, the subroutine computes the inductive part of the current subtracting geometrically the computed above resistive rms component form the total measured rms no-load current.

Determined in angle domain inductive and resistive current components are stored in separate vectors of the length 256 points each. Next, a DFT function available in DPL is applied to the vectors, and the resultant harmonic magnitudes and phase angles are geometrically added and assigned to a current source. This current source shall inject the calculated harmonic currents into the investigated network during harmonic load flow studies.

4. VERIFICATION

The implemented algorithm has been verified first with the example data provided in the original paper [7]. The results were identical as in [7], which means that the algorithm has been implemented correctly. This verification process is presented in detail in [10]. In this paper an additional verification has been performed, against own, real-world harmonic measurements performed on a single-phase transformer. The no-load test was performed. The voltage has been changed in the range form 0.1 p.u. up to 1.3 p.u. and the following values have been measured: sinusoidal supplying voltage U_{rms}, no-load current I_{rms}, harmonic distortion of the no-load current, harmonics 3rd, 5th, 7th, 9th, 11th, 13th, no-load losses P_0. Next, the measured no-load current and no-load losses were used as input data for the implemented algorithm. Determined piecewise linear resistance R and inductance L are shown in Figure 5. The resultant inductive and resistive current components for saturated core (U = 1.3 p.u.) are shown in Figure 6. Figure 7 shows the content of no-load current harmonics versus exciting voltage. It can

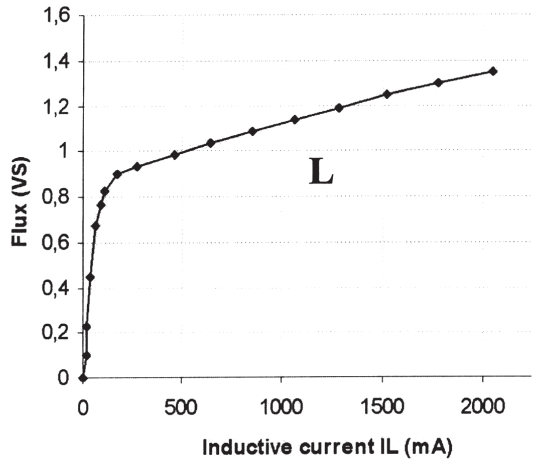

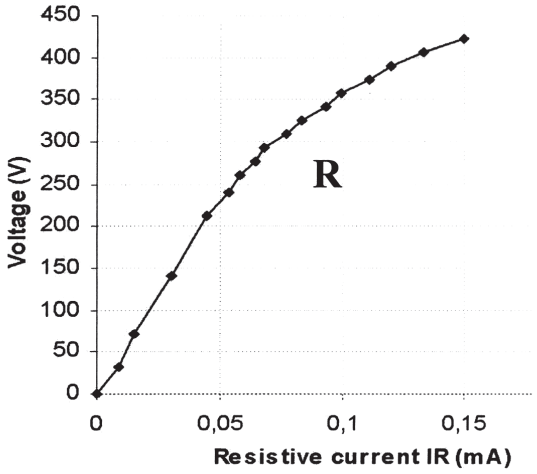

Fig. 5. Determined piecewise linear inductance L and resistance R

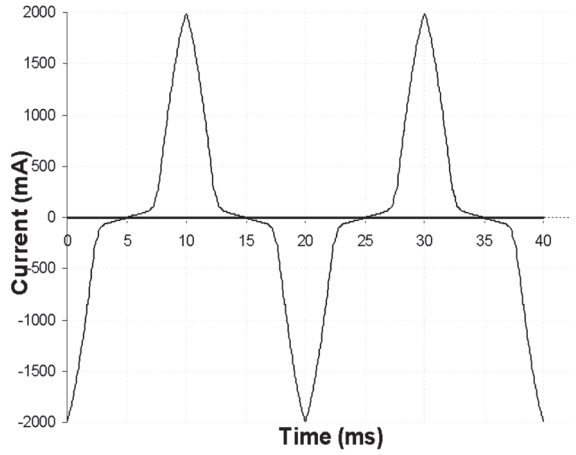

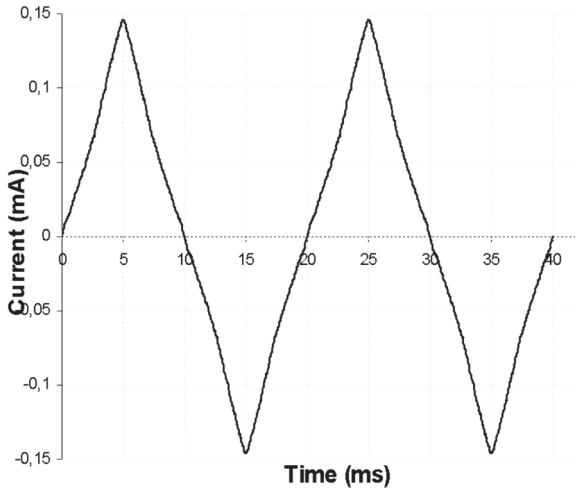

Fig. 6. Inductive (left) and resistive (right) current components determined by the algorithm. Core saturated (U = 1.3 p.u.)

be seen that the variation of the no-load current harmonics versus exciting voltage measured and determined using the algorithm is comparable, especially for a heavily saturated core. However higher order harmonics show better agreement with the measured values than lower order harmonics.

5. THREE-PHASE TRANSFORMERS

5.1. Three-limb three-phase transformer

Now, a case where three, single-phase transformers are combined, to create a three-limb transformer but with all three windings supplied with the same sinusoidal (zero-sequence) voltage U_1 is considered, see Figure 8a. The resultant fluxes will have the same direction in all three legs, and therefore they will be pushed-out of the ferromagnetic core and run in the air, oil, tank walls, etc. The magnetic permeability of the air or oil μ_{air} is much lower than the permeability of the ferromagnetic core μ, and therefore the resultant zero-sequence flux Φ_{air} will be much lower than the positive/negative sequence flux Φ. This in turn means that the zero-sequence equivalent core inductance L'_m is much smaller than the positive/negative sequence inductance Lm, where the voltages and resultant fluxes, shifted with respect to each other by 120 deg run entirely in the magnetic core, see Figure 8b. Moreover the zero-sequence inductance L'_m probably may be assumed linear, because the flux practically depends on the linear air/oil permeability, and the flux will be reduced because of the higher equivalent reluctance, which will cause the core to be less saturated. For the same reason the zero-sequence core losses may be ignored.

Therefore, justified would be the assumption that for three-leg transformers, the magnetizing current caused by the zero-sequence, sinusoidal voltage is also sinusoidal. Besides, it can be concluded that even if the magnitudes of supplying voltages are the same in both cases 8a and 8b, the magnetizing current in case 8a will be larger than in case 8b. If the flux Φ_{air} would run entirely in the air, the resultant equivalent inductance would have similar value like the leakage inductance of the primary winding L_{HV}. In reality the fluxes still enter the core and therefore the inductance L'_m is several times higher than the leakage inductance of the windings $L_{HV} < L'_m << L_m$ [6]. In case 8b, the three-phase sinusoidal

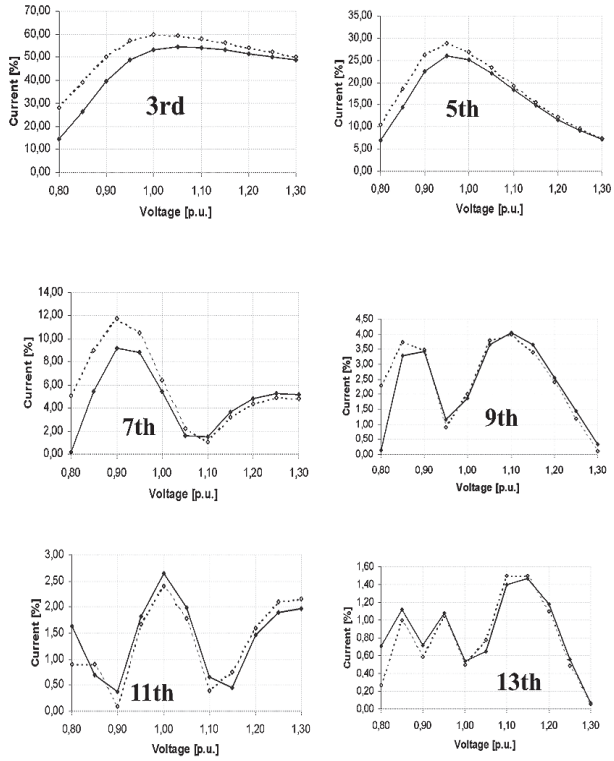

Fig. 7. No-load current harmonics versus exciting voltage. Dotted line – measured values, continuous line – calculated using the algorithm

voltage will create a three-phase sinusoidal flux that will run entirely in the core. The consequence is that the flux will pass only through the material that is characterized by a high and nonlinear value of permeability μ, and the magnetizing current will be nonlinear in the same way like in the case of a single-phase transformer (ignoring core asymmetries that introduce coupling between sequences).

5.2. Effect of winding connections

The analysis presented above was made with the assumption that the primary winding is connected in grounded star, so the impedance for all harmonics is $\boldsymbol{Z}$. In that case the magnetizing current will contain all odd harmonics including that of the zero-sequence, which are the 3rd, the 9th, 15th, etc. If the grounding of the starpoint is removed, the impedance $\boldsymbol{Z}$ for all zero-sequence harmonics would become infinitely large, which means that the triplen current harmonics will be blocked, see Figure 9. Since (5) must be always true, the blocked triplen current harmonics will cause the magnetic flux and the voltage at the winding terminals to be distorted. This is a very undesirable phenomenon. The zero-sequence flux components will be pushed out of the core (this will result in the lower magnitude of the flux, due to the higher reluctance) and this flux will in turn induce back zero-sequence voltage in the primary winding.

Therefore, a power transformer connected in ungrounded Wye (with no delta connected winding) if exposed to saturation will produce zero-sequence harmonic voltages. This voltage distortion can be modelled as a voltage source connected across the transformer terminals, see Figure 9.

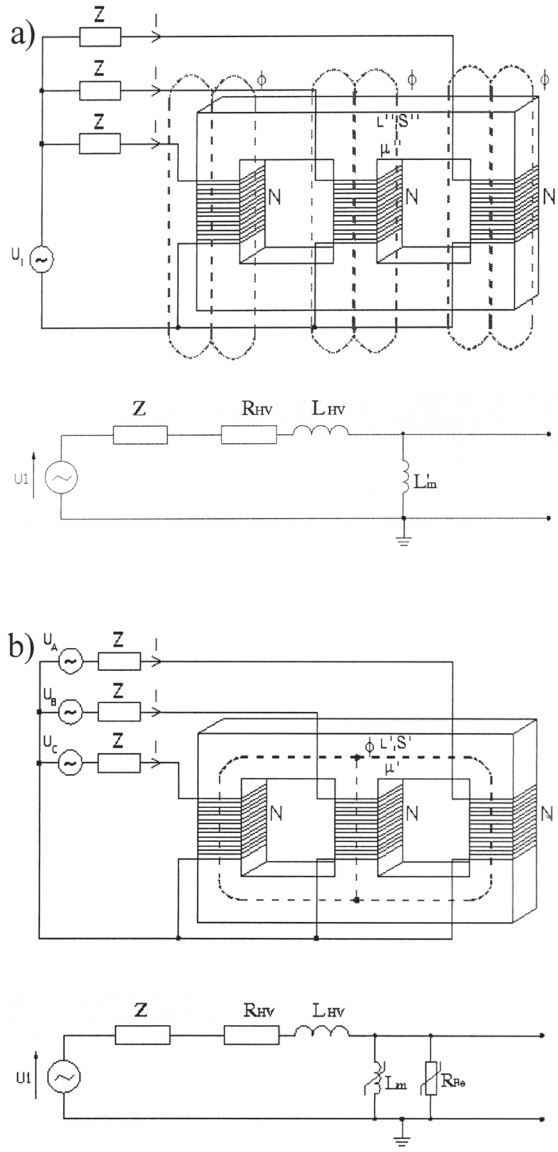

Fig 8. Three-phase transformer supplied with a) purely zero-sequence voltage U_1 and its equivalent circuit, b) three-phase positive sequence voltages U_A, U_B, U_C, and its equivalent circuit

In this figure, the equivalent diagrams for the fundamental and higher frequencies of the positive, negative and zero-sequence harmonics are shown, for two transformer winding arrangements: *Yy* and *Yd*. When looking at the equivalent diagram, the advantage of including a winding connected in delta becomes apparent. If the starpoint of the primary winding is isolated, winding connected in delta will provide the only path for zero-sequence currents generated by the core. Therefore, the presence of a delta winding will prevent the transformer from distorting the supplying voltage with zero-sequence harmonics. A power system can usually cope with relatively high levels of current distortion. Bearing in mind that the measure of power quality in a power system is actually the voltage quality [4], it can be emphasized that the distorted current does not have the direct influence on the power quality – it must be first coupled by the system impedance *Z*, and then, by the created harmonic voltage drops

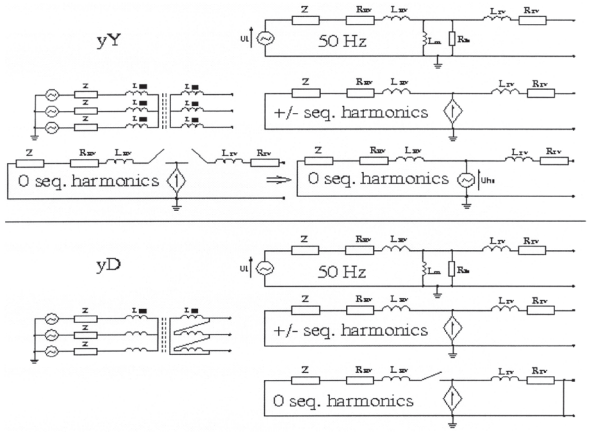

Fig. 9. Equivalent diagrams of transformers connected in a) *yY* and b) *yD*

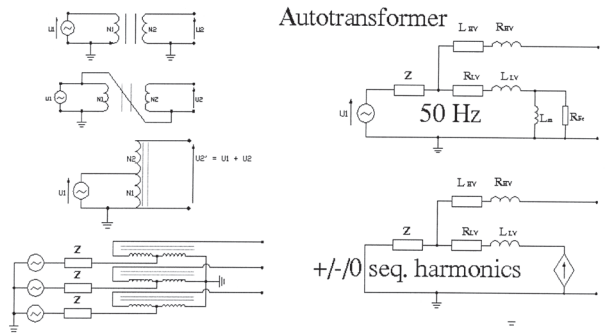

Fig. 10. Process of creating the equivalent diagram of an autotransformer, which is useful for harmonic analysis

it will affect the power quality. All the harmonics for which the diagrams are valid are created within the transformer, due to the saturation. It shall be also stated that the 4 or 5-legged transformers will behave principally like single-phase transformers – the flux will always have a return path through the core. There can be small differences noticed for each phase due to the core asymmetries.

5.3. Restrictions when using the algorithm for three-phase transformers

The described in this paper algorithm works for single-phase transformers. However, under certain circumstances it can be used also for modelling the nonlinearities of three-phase power transformers. From the theoretical analysis arises that the following restrictions regarding the no-load tests shall apply:

— The three-phase transformer must be supplied through a star connected winding YN,
— The starpoint of this primary winding shall be grounded (YN) because otherwise all triplen harmonics will be blocked,
— The voltage source that is used for supplying the transformer must be connected in grounded star YN.
— Delta connected winding shall not be used as primary because the triplen harmonics will circulate in the winding and will not be present in the measured current,
— Also none of the secondary windings shall be connected in delta. This can be deducted from the equivalent diagram shown on Figure 9. The zero-sequence harmonic currents originating in the core will split and flow into the supplying winding *Yn*, any other winding connected in grounded star yn terminated with a load impedance connected in *YN*, or any winding connected in delta.

It does not matter if the transformer core is 3, 4 or 5-legged, because the supplying voltage and the resulting flux in the core is sinusoidal and purely positive sequence. No zero-sequence flux will appear due to the core nonlinearity because the supplying winding is connected in grounded star.

5.4. The autotransformer

The main difference between a regular transformer and an autotransformer is that the autotransformer has the primary and secondary windings connected in the way that the voltage drop on the primary winding rises the potential of the secondary winding, see Figure 10.

Therefore, the secondary voltage to ground is the sum of the voltage drops on the primary and secondary coils. By raising the voltage, the power that can be transferred through the transformer is higher. However, this operation removes the galvanic insulation between the windings. There is also a difference for the *dc* component. The *dc* current is not transferred through a regular transformer while in a autotransformer it will split and the major part will close through the resistance of the primary winding and the remaining part can flow into the secondary side, depending on the *dc* (zero-sequence) resistance of the loads. The no-load testing procedure performed on an autotransformer does not differ from the procedure applied when testing a regular transformer. If the transformer is supplied with nominal voltage, the resultant flux density in the core has also its nominal value, whichever winding is used as the primary. The core nonlinearity of power autotransformers can be modelled using the described algorithm if they comply with the restrictions described for regular three-phase power transformers. The autotransformers installed in the Energinet.dk power system are *YNyn* connected and some of them have an additional tertiary winding. However, this winding is normally not used and therefore, it is connected in open delta. Consequently it will not affect the flow of harmonic currents because no current can circulate and they cannot produce opposing flux. Consequently it can be concluded that if three-phase power autotransformers comply with the restrictions described in section V.C, the algorithm can be used for modelling their core nonlinearities.

6. SUMMARY AND CONCLUSIONS

— It is possible to implement the algorithm in the PowerFactory simulation software,
— The algorithm has been verified first against the original data provided in [7] and the agreement was perfect, which proves that the algorithm has been correctly implemented,
— The comparison of the results with own measurements on a small single phase transformer has shown that

higher order harmonics show better agreement with the measured values than lower order harmonics,
— A difference in the measured and calculated 3rd harmonic content in the no-load current, for low exiting voltage (0.8 – 0.9 p.u.) has been noticed but the reason for this has not been revealed,
— Based on the performed theoretical analysis it can be stated that the algorithm initially valid for single-phase transformers can be used for modelling nonlinearities of three-phase autotransformers, however verification with measurements would be desirable,
— The algorithm allows assessing the levels of harmonic distortion due to the aggregated effect of power autotransformers on the harmonic levels in the Danish transmission grid.

7. FUTURE WORK

Tat the most important future task shall be to verify the implemented algorithm with precise measurements on full-size power autotransformers.

ACKNOWLEDGEMENT

The authors wish to gratefully acknowledge the valuable assistance of M. Pöller and E. Zimmermann from DIgSILENT GmbH.

REFERENCES

1. Arrillaga J., Watson N.R.: *Power System Harmonics*. John Willey & Sons, London, 2003, p. 62–64.
2. Chua L.O., Stromsmoe K.A.: *Lumped Circuit Models for Nonlinear Inductors Exhibiting Hysteresis Loops*. IEEE Trans. On Circuit Theory, CT-17, 4, Nov. 1970, pp. 564–574.
3. Dommel H.W.: *Electromagnetic Transients Program Reference Manual (Section 6)*. Bonneville Power Administration, Portland, Oregon, December 1999.
4. Dugan R.C., McGranaghan M.F., Santoso S. and Beaty H.W.: *Electrical Power Systems Quality.* McGraw-Hill, New York, 2002.
5. Dugui W., Zheng X.: *Harmonic model of power transformer*. 1998. In Proc. POWERCON '98, 1998, International Conference on Power System Technology, 18–21 Aug. 1998, pp. 1045 – 1049.
6. Bolkowski S.: *Electric Circuit Theory (in Polish)*. WNT, Warsaw, 1995, p. 196.
7. Neves L.A.N., Dommel H.W.: *On Modelling Iron Core Nonlinearities*. IEEE Transactions on Power Systems, Volume 8, Issue 2, May 1993, Page(s): 417–425.
8. PowerFactory Manual, PowerFactory Manuals, ver. 13.1, 2005.
9. Santesmases J.G., Ayala J., Cachero S.H.:*Analytical Approximation of Dynamic Hysteresis Loops and its Application to a Series Ferroresonant Circuit.* Proc. IEE 117, January 1970, pp. 234–240.
10. Wiechowski W.: *Harmonics in Transmission Power Systems*. PhD dissertation, Aalborg University, Denmark, 2006, ISBN 978-87-89179-69-8.

Wojciech Wiechowski
received the M.Sc. degree from Warsaw University of Technology in 2001 and the Ph.D. degree from Aalborg University, Denmark in 2006. From 2001 to 2002 he worked for HVDC SwePol Link as a Technical Executor. In the period from 2002 to 2006 he was with the Institute of Energy Technology, Aalborg University, first as a PhD Student and later as an Assistant Professor. Since 2006 he has been employed in the Planning Department of the Danish TSO Energinet.dk. His current responsibilities include various power system analyses related to the planning of the transmission network with extensive use of long AC cable links and wind power generation. He is a Senior Member of IEEE.

Birgitte Bak-Jensen
was born in Grenaa, Denmark, on August 27, 1961. She received the M.S. degree in electrical engineering and the Ph.D. degree in modeling of high-voltage components from Aalborg University, Aalborg East, Denmark, in 1986 and 1992, respec-tively. From 1986 to 1988, she was with Electrolux Elmotor A/S, Aalborg East, Denmark, as an Electrical Design Engineer. She is an Associate Professor in the Institute of Energy Technology, Aalborg University, where she has worked since August 1988. Her fields of interests are modeling and diagnosis of electrical components in power systems, power quality, dispersed generation and stability in power systems with large integration of wind power.

Claus Leth Bak
was born in Århus in Denmark, on April 13, 1965. He graduated from High School in Århus and studied at the Engi-neering college in Århus, where he received the B.Sc. with honours in Electrical Power Engineering in 1992. He pursued the M.Sc. in Electrical Power Engineering with specialization in High Voltage Engineering at the Institute of Energy Technology (IET) at Aalborg University (AAU), which he received in 1994. After his studies he worked with Electric power transmission and substations with spe-cializations within the area of power system protection at the NV Net company. In 1999 he got employed as an assistant professor at IET-AAU, where he is holding an associate professor position today. His main research areas include corona phenomena on overhead lines, power system transient simulations and power system protection. Main teaching areas are high voltage technology, power system analysis and simulation, relay protection and electrophysics. He works as a consultant engineer for electric utilities, mainly in the field of power system protection and power system analysis.

Jan Lykkegaard
was born in Denmark in 1968. He received the M.Sc. degree in electrical engineering in 1994 from Institute of Energy Technology, Aalborg University. From 1995 to 1999 he was employed at Elsam. Since 1999 he has been working in the Substation Department of the Danish Transmission System Operator Energinet.dk. His main responsibilities include transmission transformers, shunt reactors and various R&D tasks.